

# ACCRETION DISK TEMPERATURES AND CONTINUUM COLORS IN QSOS

E. W. BONNING

Laboratoire de l'Univers et de ses Théories, Observatoire de Paris, F-92195 Meudon Cedex, France

AND

L. CHENG, G. A. SHIELDS, S. SALVIANDER, K. GEBHARDT  
 Department of Astronomy, University of Texas, Austin, TX 78712  
*Submitted to The Astrophysical Journal*

## ABSTRACT

Accretion disks around supermassive black holes are widely believed to be the dominant source of the optical-ultraviolet continuum in many classes of active galactic nuclei (AGN). We study here the relationship between the continuum colors of AGN and the characteristic accretion disk temperature ( $T_{\max}$ ). Based on NLTE models of accretion disks in AGN computed as described by Hubeny et al. (2000), we find that continuum intensity ratios for several pairs of wavelengths between 1350 and 5100 Å should show a trend of bluer colors for higher  $T_{\max}$ , notwithstanding random disk inclinations. We compare this theoretical expectation with observed colors of QSOs in the Sloan Digital Sky Survey (SDSS), deriving black hole mass and thence  $T_{\max}$  from the width of the Mg II broad emission line. The observed colors generally do not show the expected trend and in some cases show a reverse trend of redder colors with increasing  $T_{\max}$ . The cause of this discrepancy does not appear to be dust reddening or galaxy contamination but may relate to the accretion rate, as the offset objects are accreting above  $\sim 30\%$  of the Eddington limit. The derived disk temperature depends primarily on line width, with little or no dependence on luminosity.

*Subject headings:* galaxies: active — quasars: general — black hole physics

## 1. INTRODUCTION

Accretion onto supermassive black holes is widely accepted as the energy source of AGN. Much of the optical and ultraviolet luminosity, specifically the so-called “Big Blue Bump” may be thermal emission from an accretion disk (Shields 1978; Malkan 1983; for a review of attempts to relate disk models to QSO spectra see Koratkar & Blaes 1999). In the simplest picture, radiation from each radius in the disk is powered by energy produced locally by viscous dissipation within the vertical thickness of the disk. Models achieve some success in fitting the spectral energy distribution (SED) of individual QSOs (e.g., Sun & Malkan 1989; Blaes et al. 2001; and references therein). Simple disk models nevertheless have shortcomings (e.g., Antonucci 1999). Time variations of the optical, ultraviolet, and X-ray continuum of some AGN show patterns suggestive of reprocessing in an externally illuminated atmosphere (Collin 1991). Polarization of the optical continuum of QSOs is weaker in degree and opposite in sign from that expected from a smooth electron scattering atmosphere (see Coleman & Shields 1990, and references therein). The soft X-ray continuum cannot be explained by ordinary thermal emission from the disk atmosphere, and requires another ingredient such as a Compton-scattering corona (Wilkes & Elvis 1987; Comastri et al. 1992; Blaes et al. 2001). On the other hand, Kishimoto et al. (2005) argue from spectropolarimetry that the infrared continuum of AGN accretion disks has a slope similar to that expected from simple disk models.

The mixed success of the disk model makes it important to explore further tests of the basic agreement between the model and observations. One simple test involves the temperature of the disk and the expected color

of the continuum. Wien’s law suggests that hotter disks should in general have bluer continua. This is born out by models, as we discuss below. The disk effective temperature varies with radius in a self-similar way, and the temperature of a given disk can be parameterized by the maximum value of the local effective temperature,  $T_{\max} \propto L_{\text{bol}}^{1/4} M_{\text{BH}}^{-1/2}$ , that occurs at a radius slightly outside the inner disk boundary (see review by Novikov & Thorne 1973).  $T_{\max}$  varies with  $M_{\text{BH}}$  and the accretion rate  $\dot{M}$  as  $T_{\max}^4 \propto \dot{M}/M_{\text{BH}}^2$ , because the bolometric luminosity ( $L_{\text{bol}}$ ) is proportional to  $\dot{M}$  and the disk radius scales with the gravitational radius  $R_g = GM/c^2$ . One consequence is that, for objects shining at a given fraction of the Eddington limit ( $L_{\text{Ed}} \propto M_{\text{BH}}$ ), the temperature decreases with increasing luminosity or mass. On this basis, one might expect luminous QSOs to have softer (redder) continuum slopes than lower luminosity AGN. This expectation is not consistently fulfilled by observed SEDs of AGN. There is a trend of increasing soft X-ray excess with narrower H $\beta$  and higher Eddington ratio (e.g., Laor et al. 1997); these quantities correlate in practice with higher  $T_{\max}$ . The “Baldwin effect”, which involves decreasing emission-line equivalent width for higher luminosity, is also consistent (Wandel 1999; Dietrich et al. 2002). More luminous objects should have cooler disks and softer ionizing continua. Scott et al. (2004) find harder EUV slopes for higher  $M_{\text{BH}}$  and luminosity, although curiously the trend is largely lost in scatter in their plot of slope versus  $T_{\max}$ . Blaes (2003), looking at continuum slope as a function of  $M_{\text{BH}}$  and  $L/L_{\text{Ed}}$  for a small set of AGN, found a large degree of scatter but an overall trend apparently opposite to theoretical expectation (also noted by Cheng, Shields, & Gebhardt 2004).

$T_{\max}$  may be estimated for individual objects with knowledge of  $M_{\text{BH}}$  and  $\dot{M}$ . The accretion rate can be estimated from the bolometric luminosity, and  $M_{\text{BH}}$  can be estimated with the aid of recently established methods utilizing the widths of the broad emission lines (Kaspi et al. 2000, 2005; Bentz et al. 2006). In this paper, we use spectra from the SDSS DR3<sup>1</sup> to examine the continuum slope of QSOs as a function of  $T_{\max}$ . In Section 2, we describe the theoretical models we use and compare them to observed QSOs. Results are discussed in Section 3.

## 2. MODELING AND DATA SAMPLING

### 2.1. Accretion Disk Properties

The Eddington limit for a black hole (BH) with mass  $M_{\text{BH}}$  is given by

$$L_{\text{Ed}} = \frac{4\pi c G M_{\text{BH}}}{\kappa_e} = (10^{46.10} \text{ erg s}^{-1}) M_8, \quad (1)$$

where  $\kappa_e$  is the electron scattering opacity per unit mass and  $M_8 = M_{\text{BH}}/(10^8 M_\odot)$ . The disk luminosity production through accretion onto the black hole is

$$L = \epsilon \dot{M} c^2 = (10^{45.76} \text{ erg s}^{-1}) \epsilon_{-1} \dot{M}_0. \quad (2)$$

where  $\dot{M}_0$  is the accretion rate in  $M_\odot \text{ yr}^{-1}$ , and  $\epsilon = 10\epsilon_{-1}$  is the efficiency. For a Schwarzschild (non-rotating) black hole,  $\epsilon = 0.057$ , and for a rapidly rotating Kerr hole with angular momentum parameter  $a_* = 0.998$ ,  $\epsilon = 0.31$  (Novikov & Thorne 1973). The effective temperature at radius  $r$  is given by the local radiative flux leaving the atmosphere,  $T_{\text{eff}} = (F/\sigma)^{1/4}$ . For  $a_* = 0.998$  (Thorne 1974),

$$T_{\max} = (10^{5.56} \text{ K}) M_8^{-1/4} (L_{\text{bol}}/L_{\text{Ed}})^{1/4}, \quad (3)$$

or alternatively,  $T_{\max} = (10^{5.54} \text{ K}) M_8^{-1/2} L_{46}^{1/4}$ , where  $L_{46} \equiv L_{\text{bol}}/(10^{46} \text{ erg s}^{-1})$ . For a Schwarzschild hole,  $T_{\max}$  is cooler by a factor of  $10^{0.46}$  for a given  $M_{\text{BH}}$  and  $L_{\text{bol}}$  (e.g., Shields 1989).

In traditional treatments, the local vertical structure is determined by hydrostatic equilibrium and radiative and convective transport of heat produced locally by viscous stresses. The viscosity also determines the radial diffusion of matter and the surface density of matter in the disk as a function of radius. The locally emitted spectrum is determined by  $T_{\text{eff}}$  and the effective gravity in the atmosphere. The locally emitted spectrum shows strong features such as the Lyman edges of hydrogen and helium, but in the observed spectrum these features are broadened by relativistic effects.

### 2.2. Deriving $M_{\text{BH}}$ and $T_{\max}$

Derivation of  $M_{\text{BH}}$  from the width of the  $\text{H}\beta$  or  $\text{Mg II}$  broad emission lines has become widely accepted in recent years. The FWHM of the broad lines is taken to give the circular velocity of the broad-line emitting material (with some geometrical correction factor). The radius of the broad-line region (BLR), derived from echo mapping studies, increases as a function of the continuum luminosity,  $R \propto L^\Gamma$  with  $\Gamma = 0.5 - 0.7$  (Wandel et al. 1999; Kaspi et al. 2000, 2005). Simple considerations involving photoionization physics suggest  $\Gamma = 0.5$  (Shields et

al. 2003). Bentz et al. (2006) find  $\Gamma = 0.52 \pm 0.04$  after correcting the sample of Kaspi et al. (2005) for host galaxy contamination. Such studies typically use the  $\text{H}\beta$  broad line, but McLure & Jarvis (2002) find that the  $\text{Mg II } \lambda 2800$  line is a valid alternative useful at higher redshifts. Here we use the expression for  $M_{\text{BH}}$

$$M_{\text{BH}} = (10^{7.69} M_\odot) v_{3000}^2 L_{44}^\Gamma, \quad (4)$$

where  $v_{3000} \equiv \text{FWHM}/3000 \text{ km s}^{-1}$ ,  $\Gamma = 0.5$ ,  $L_{44} \equiv \lambda L_\lambda(5100)/(10^{44} \text{ erg s}^{-1})$ , and the coefficient is taken from Shields et al. (2003). We use the FWHM of the  $\text{Mg II}$  line in order to get maximum coverage in redshift for a single broad emission line.

The derived value of  $T_{\max}$  depends almost entirely on the the broad line FWHM for a given object. The bolometric luminosity can be estimated as  $L_{\text{bol}} = f_L \times \lambda L_\lambda(5100)$ , following Kaspi et al. (2000). Using Eq. 4 and this expression for  $L_{\text{bol}}$ , Eq. 3 becomes

$$T_{\max} = (10^{5.43} \text{ K}) v_{3000}^{-1} L_{44}^{-(\Gamma-0.5)/2} (f_L/9)^{-1/4}, \quad (5)$$

Note that for  $\Gamma = 0.5$ , as used here, the derived disk temperature is inversely proportional to FWHM with no dependence on  $L$ , save the bolometric correction factor  $f_L = 9$  (Kaspi et al. 2000). Shang et al. (2005), in an analysis of the SEDs of 17 well observed QSOs, also adopted  $f_L = 9$ , although their broad band SEDs typically indicate a larger value, on average  $f_L \approx 13$ . More recently, Richards et al. (2006) find an average bolometric correction from 5100 Å of  $\sim 10$  from composite SEDs of 259 QSOs. We discuss the sensitivity of our results to the value of  $f_L$  in Sec. 3.1 below.

### 2.3. The Color- $T_{\max}$ Relation from the Non-LTE Models

One might expect that cooler disks will in general have redder colors. This certainly would be true (apart from inclination effects) for non-relativistic disks emitting locally as black bodies. However, disks in AGN are expected to depart from black body emission locally, and the energy distribution received by a particular observer is strongly affected by relativistic effects. The observer's angle  $i$  with respect to the disk axis is also important, because the radiation from the innermost, hottest part of the disk will be relativistically beamed near the equatorial plane, especially for rapidly rotating holes (Cunningham 1975; Laor & Netzer 1989). Therefore, models are needed to establish the expected statistical relationship between  $T_{\max}$  and color. In recent years, I. Hubeny and his colleagues have computed NLTE disk models for AGN and made comparisons with observation (Hubeny et al. 2000). Hubeny et al. have kindly made available the computer program AGNSPEC which gives the observed energy distribution ( $4\pi dL_\nu/d\Omega$ ) emitted in the observer's direction for model disks as a function of  $M_{\text{BH}}$ ,  $\dot{M}$ ,  $a_*$ , inclination, and the Shakura & Sunyaev (1973) viscosity parameter  $\alpha$ . The vertical structure and local emission is evaluated at each radius in the disk, and the spectrum viewed at infinity is calculated via the general relativistic transfer function. Using AGNSPEC, we computed a set of models with values of  $M_{\text{BH}}$  and  $\dot{M}$  representative of our SDSS QSO sample (discussed below). We select the range of  $\dot{M}$  to give Eddington ratios consistent with those in our observed sample (see Fig. 7

<sup>1</sup> The SDSS website is <http://www.sdss.org>.

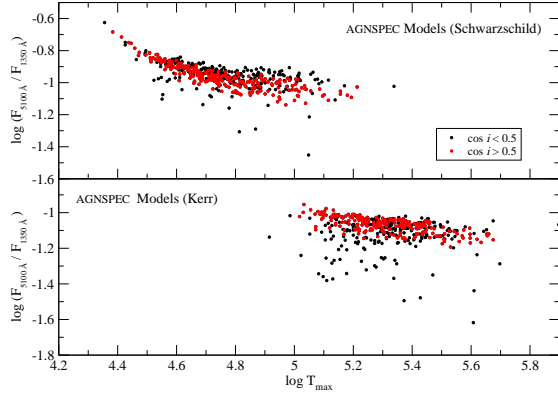


FIG. 1.— Continuum flux ratio  $F_{\lambda}(5100)/F_{\lambda}(1350)$  for Schwarzschild and Kerr black holes. The Schwarzschild models are cooler because they were computed for the same set of values of  $M_{\text{BH}}$  and  $L_{\text{bol}}$ . The points show an overall trend of bluer colors with increasing  $T_{\text{max}}$ . Models with high inclination ( $\cos i < 0.5$ , black dots) show more scatter due to the relativistic effects on edge-on disks.

and discussion below. We fix  $\alpha = 0.10$  and, except as noted below,  $a_* = 0.998$ . Hubeny et al. (2000) show that models with  $\alpha = 0.1$  and  $0.01$  differ negligibly at the wavelengths of interest here. To assess the effect of disk inclination on the observed colors, we assign a random inclination (uniform distribution in  $\cos i$ ) to each model.

In Fig. 1 we plot the luminosity ratio  $L_{\lambda}(5100 \text{ \AA})/L_{\lambda}(1350 \text{ \AA})$  vs.  $T_{\text{max}}$ . We distinguish models with  $\cos i > 0.50$ . This is a plausible lower limit to the inclination angle for observable quasars if the “unified” model of AGN, involving an obscuring torus, applies to our QSOs (Antonucci & Miller 1985). There exists a clear overall trend wherein the spectra become more blue with increasing disk temperature, consistent with intuition. The models with  $\cos i < 0.50$  add more scatter, since relativistic beaming and Doppler shift effects result in more flux at shorter wavelengths. However, the overall trend of bluer color with increasing  $T_{\text{max}}$  is still evident. We include models for non-rotating black holes for the same  $M_{\text{BH}}$  and  $L_{\text{bol}}$  as the Kerr models. These have lower  $T_{\text{max}}$  by 0.46 dex for given color with  $T_{\text{max}}$ .

#### 2.4. The Color- $T_{\text{max}}$ Relation from the SDSS Datasets

We examined the color (i.e., continuum flux ratios) of SDSS QSOs as a function of  $T_{\text{max}}$  derived from the FWHM of Mg II as in Eq. 5 (see Sec. 2.2). The SDSS spectra cover a wavelength range of  $\lambda 3800$  to  $\lambda 9200 \text{ \AA}$ . The rest-frame colors measured for our sample are  $r_{54} \equiv F_{\lambda}(5100)/F_{\lambda}(4000)$ ,  $r_{42} \equiv F_{\lambda}(4000)/F_{\lambda}(2200)$ , and  $r_{21} \equiv F_{\lambda}(2200)/F_{\lambda}(1350)$ . The objects have redshifts between  $z \sim 0.38$  and  $z \sim 2.0$ , such that Mg II lies well within the SDSS spectrum. The broad Fe II emission blends were removed with the aid of templates in the optical and UV bands (Marziani et al. 2003 and Vestergaard & Wilkes 2001, respectively). Continuum fluxes were computed by taking the mean (biweight) value of the flux over a  $30 \text{ \AA}$  window centered on the wavelength of interest. The chosen wavelengths are relatively unaf-

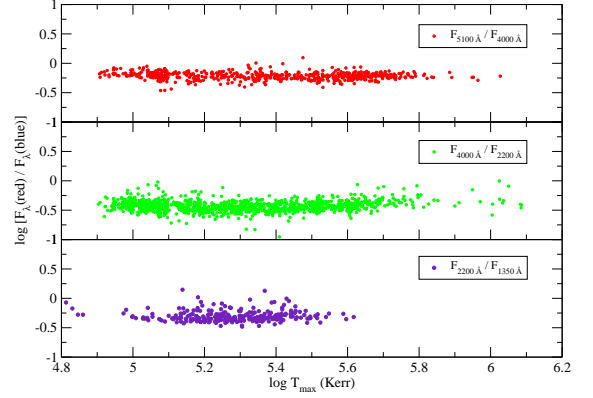


FIG. 2.— Observed continuum colors for individual QSOs as given by flux ratios at three pairs of wavelengths. The abscissa is  $\log T_{\text{max}}$  derived as described in the text, on the assumption of a rapidly rotating black hole.

ected by Fe II emission. The FWHM of the broad Mg II  $\lambda\lambda 2796, 2803$  doublet was measured by means of a least squares fit of a Gauss-Hermite function (Pinkney et al. 2003) to the line profile, together with a linear fit to the continuum in the vicinity of the line. Fits were accepted if the line widths and equivalent widths had an accuracy better than 15% and visual inspections showed a good fit and no artifacts in the spectrum or continuum windows. For more details on the measurement procedure, see Salviander et al. (2006). Figure 2 shows the results for individual QSOs in the three wavelength ranges. The figures show substantial scatter, but overall a flat or upward trend, particularly for higher  $T_{\text{max}}$ . In order to clarify the trends, we have binned the data for each wavelength range such that there are approximately equal numbers of objects per bin of  $T_{\text{max}}$  (see Fig. 3). For a given bin, we averaged the flux ratios  $\log r_{54}$ ,  $\log r_{42}$ , and  $\log r_{21}$ , for each object for which these data exist. At longer wavelengths,  $r_{54}$  agrees fairly well with the predictions of the Kerr models. The observed  $r_{42}$  tracks the models at low  $T_{\text{max}}$  but shows a significant upturn above  $\sim 10^{5.4} \text{ K}$ . Our shortest wavelength pair,  $2200/1350 \text{ \AA}$ , disagrees with theoretical predictions even at low disk temperature, and the departure increases at higher  $T_{\text{max}}$ . The observed trend of  $r_{21}$  is nearly flat with  $T_{\text{max}}$ , not showing the ‘U’-shape seen in  $r_{42}$ . In order to display a wider wavelength range than is possible with SDSS spectra of a given redshift, we have combined the binned results for the above three pairs of wavelengths by summing the averages for  $\log r_{54}$ ,  $\log r_{42}$ ,  $\log r_{21}$  to get a total  $\log r_{51} = \log(F_{\lambda}(5100)/F_{\lambda}(1350))$ . Figure 4 shows the composite color- $T_{\text{max}}$  relation for the wavelength range  $5100 - 1350 \text{ \AA}$  as well as this luminosity ratio for individual models calculated as described in Sec. 2.3. Over this wide wavelength trend, the models show a substantial trend toward bluer colors with increasing temperature. At low  $T_{\text{max}}$ , there is rough agreement between the observations and models, whereas at higher temperatures, the observed colors remain fairly constant and depart increasingly from the models. Richards et al. (2003) find a trend of narrower of  $H\beta$  with redder continuum slope, consistent with our findings. They note the possible connection with black hole mass (however, they find a trend

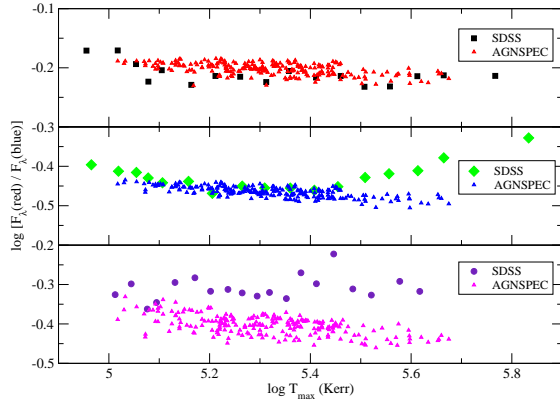


FIG. 3.— The three continuum flux ratios (5100Å/4000Å, 4000Å/2200Å, 2200Å/1350Å, as in Figure 2) averaged in bins of  $T_{\max}$  and compared with results of the disk models (assuming  $\cos i > 0.5$ ).

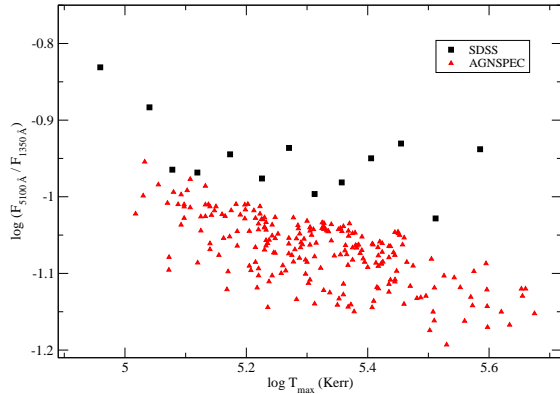


FIG. 4.— The 5100/1350 Å flux ratios for the  $\cos i > 0.5$  Kerr models together with the composite flux ratios for the SDSS objects in  $T_{\max}$  bins.

of weaker, not narrower Mg II for the same sample).

### 3. DISCUSSION

We have found that QSOs show mixed agreement with the predictions of accretion disk models as a function of disk temperature  $T_{\max}$ . We consider the three wavelength pairs  $r_{54}$ ,  $r_{42}$ , and  $r_{21}$  involving ratios of  $F_{\lambda}$  at 5100/4000, 4000/2200, and 2200/1350 Å, respectively. Accretion disk models with random inclinations show the expected trend of bluer colors with increasing  $T_{\max}$ . Observed values of  $r_{54}$  agree well with the models. For  $r_{42}$ , the observations agree with the models for  $T_{\max} < 10^{5.4}$  K, but for higher temperatures the observed colors become redder while the models become bluer. For  $r_{21}$  at low  $T_{\max}$ , the observed colors are slightly redder than the models. The observed color remains roughly constant with increasing  $T_{\max}$  while the models become distinctly bluer. Thus, for both  $r_{42}$  and  $r_{21}$ , the observed QSOs fail to show the expected trend with  $T_{\max}$ . Possible explanations of this discrepancy might include erroneous values of  $M_{\text{BH}}$  and  $\dot{M}$ , host galaxy contamination, dust reddening, and inadequacy of the disk models.

#### 3.1. Reliability of disk parameters

The derived values of  $T_{\max}$  depend on  $M_{\text{BH}}$  and  $\dot{M}$ . Values of  $M_{\text{BH}}$  from echo measurements of the BLR radius (Kaspi et al. 2005, and references therein) agree with host galaxy velocity dispersions (Gebhardt et al. 2000b; Nelson 2000). Comparison of black hole masses from an expression like Eq. 4 with host galaxy luminosities and velocity dispersion  $\sigma_*$  indicates that  $M_{\text{BH}}$  is reliable in the mean to  $\sim 0.1$  dex with a dispersion of  $\sim 0.4$  dex in individual objects (McLure & Dunlop 2002; Greene & Ho 2005). The resulting scatter of 0.2 dex and zero-point uncertainty of 0.05 dex in  $T_{\max}$  does not significantly affect our conclusions.

More difficult to assess is the uncertainty in  $\dot{M}$ . We used our disk models to assess the error introduced from using a constant bolometric correction  $f_L = L_{\text{bol}}/\lambda L_{\lambda}(5100)$  over our range of  $T_{\max}$ . The true bolometric luminosity is given by  $\dot{M}$  and  $\epsilon$  for the assumed black hole spin. We find that the model-derived  $f_L$  generally exceeds 9 in a way dependent on inclination angle. For Kerr holes, taking only inclination angles of less than  $60^\circ$ , we find values of  $f_L$  ranging up to  $\sim 80$ . On average, our assumed  $f_L$  of 9 underestimates the true value of  $f_L$  by  $\sim 0.4$  dex. Models with very small  $\cos i$  can have values of  $f_L$  of up to  $\sim 200$ -300. Such objects should have a much higher  $T_{\max}$  than we have assigned; but if such QSOs can be observed at all, they will represent only a small number of objects. Since the bolometric correction factor enters into the formula for  $T_{\max}$  in the one-fourth power, the effect of an average 0.4 dex underestimation of the luminosity translates into a 0.1 dex underestimation of the temperature.

Figure 5 shows a comparison between the models of Fig. 1 and those same models with  $T_{\max}$  computed from  $L_{\text{bol}} = 9 \times \lambda L_{\lambda}(5100)$ . The effect of underestimating  $L_{\text{bol}}$  for objects of low inclination is slight, as noted above. The effect of significant underestimation of  $L_{\text{bol}}$  for high inclination objects is evident. These objects'  $T_{\max}$  are far too low compared with their true temperatures. While these objects do show a trend of increasing red color with  $T_{\max}$ , this only manifests at low  $T_{\max}$  and only in objects of high inclination. Our discussion has mostly assumed a near-extremal Kerr black hole ( $a_* = 0.998$ ). It is not known what the black hole spin distribution is in quasars; the spin parameter is dependent on the merger history of the black holes (which tends to decrease the spin) and the gas accretion history (which will spin up the accreting black hole). It is expected to range from  $\sim 0.6$  up to about  $a_* = 0.9$  (see, e.g. Volonteri et al., 2005; Gammie, Shapiro, & McKinney, 2004; Hughes & Blandford 2003). The effect of assuming a variety of spins for our observations would be to lower  $T_{\max}$  by up to 0.46 dex (for a zero spin black hole). This may serve to more closely align the lower temperature bins with the models, but only increases the discrepancy of the observations at higher  $T_{\max}$ . Uncertainties in  $T_{\max}$  whether due to uncertainties in  $L_{\text{bol}}$  or overestimating the black hole spin do not seem likely to resolve the discrepancy between observed colors and disk models.

#### 3.2. Host galaxy contamination

Another contributor to QSO colors is starlight from the host galaxy. The contribution of host-galaxy light

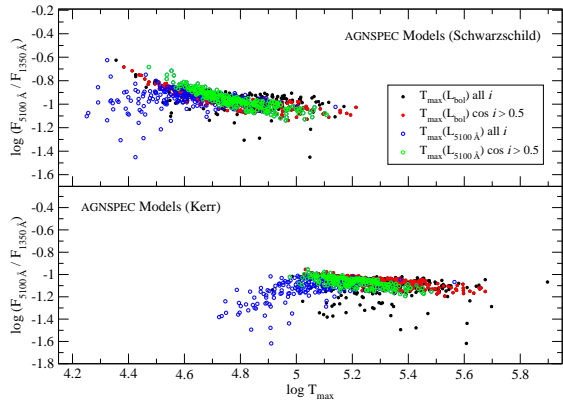


FIG. 5.— The same models as computed for Fig. 1 but with  $T_{\max}$  computed from the model spectrum using  $L_{\text{bol}} = 9 \times \lambda L_{\lambda}(5100)$ . Disks with high inclination show significant under-estimation of  $T_{\max}$  (see discussion of  $f_L$  in text). Low inclination disks, however, retain the qualitative color v.  $T_{\max}$  trend seen when the model colors are plotted as a function of the true  $T_{\max}$ .

is indeed seen via stellar absorption lines in SDSS composite spectra (Vanden Berk et al. 2001). They find a contribution to the composite quasar continuum from stars of about 7%–15% at the locations of Ca II  $\lambda 3933$  and Na I  $\lambda 5896$  and about 30% at the locations of Ca II  $\lambda 8498$ , 8542. Studies of black holes in nearby quiescent galaxies find  $M_{\text{BH}}$  roughly proportional to galaxy luminosity (see review by Kormendy & Gebhardt 2000). If we assume  $L_{\text{gal}} \propto M_{\text{BH}}$ , we expect an increasing galaxy contribution with decreasing  $L/L_{\text{Ed}}$ . We show in Fig. 7 that for our SDSS QSOs,  $L/L_{\text{Ed}}$  increases with  $T_{\max}$ , so the galaxy contribution should make the observed QSOs increasingly redder than the models for decreasing  $T_{\max}$ , opposite to the trend that we find. Finally, we have made composite spectra for our QSO sample grouped according to  $T_{\max}$ . The Ca K line, visible but weak, suggests a galaxy contribution of only a few percent at  $\lambda 4000$ , and no perceptible difference between the objects with higher and lower  $T_{\max}$ . This suggests that host galaxy starlight does not cause the divergence of observed and model colors with increasing  $T_{\max}$ .

### 3.3. Reddening

Numerous studies have considered the degree of reddening of AGN and its wavelength dependence (e.g., Wilkes et al. 1999; Richards et al. 2003). Hopkins et al. (2004) studied the reddening in QSOs of SDSS DR1. Based on correlations of color and spectral curvature and reddening curves by Pei (1992), they conclude that the minority of objects that do show significant reddening are consistent with an SMC reddening curve but not with LMC or Galactic reddening. However, the patterns in Fig. 3 are not consistent with reddening by dust. The observed values of  $r_{42}$  follow the Kerr models below  $T_{\max} = 10^{5.4}$  K, then turn up sharply toward redder values. In contrast,  $r_{21}$  deviates from the models even at the lowest temperatures, showing roughly constant values as a function of  $T_{\max}$ . For SMC dust, the reddening of the  $r_{54}$  flux ratio is relatively small and inconclusive for our discussion. The argument is even stronger for LMC or MWG dust, for which the reddening between  $\lambda 1350$  and  $\lambda 2200$  is smaller or even negative. The Gaskell et al.

(2004) reddening curve is flat in the ultraviolet, giving similar values of differential extinction of  $r_{21}$  and  $r_{42}$ , and much less for  $r_{54}$ . Such a reddening curve cannot explain the results in Fig. 3.

We caution that the amounts of reddening required to affect the curves in Fig. 3 is not large. An increase in  $r_{21}$  of  $\sim 0.09$  dex requires  $E(B-V) = 0.03$  or  $A_V = 0.09$ ; the same change in  $r_{42}$  requires  $E(B-V) = 0.05$  or  $A_V = 0.16$ . For comparison, the amount of Galactic reddening of the SDSS QSOs used here averages about  $A_g = 0.13$  for the SDSS  $g$ -band photometric color. However, the reddening would need to correlate systematically with broad line width to explain the trends in  $r_{42}$  or  $r_{21}$ . To test this possibility, we assume that the amount of dust reddening correlates with broad line width (i.e.  $T_{\max}$ ) in such a way as to give overall agreement in the ratio  $r_{21}$ . Figure 6 shows the binned points of Fig. 3 de-reddened with an assumed reddening of  $r_{21}$  given by  $\Delta \log r_{21} = -0.57 + 0.125 \cdot \log T_{\max}$ . This is tailored in such a way as to give overall agreement between the de-reddened observations and the models for  $r_{21}$ . The SMC extinction curve (Pei 1992) gives  $\Delta \log r_{42}/\Delta \log r_{21} = 0.61$  and  $\Delta \log r_{54}/\Delta \log r_{21} = 0.16$ . The figure shows that the de-reddened  $r_{42}$  now is bluer than the models for lower  $T_{\max}$ , and at high  $T_{\max}$  it rises to redder values in a way not reflected in the models. The de-reddened  $r_{54}$  now is significantly bluer than the models for most values of  $T_{\max}$ . Evidently, reddening cannot reconcile the models and observation in detail, even for a carefully tailored increase of reddening with broad line width.

Reddening may nevertheless have a significant effect on the observed colors and their relationship to the model colors. For example, Constantin & Shields (2005) find evidence for greater reddening in Narrow Line Seyfert 1s (NLS1s) than in the AGN population as a whole. Baskin & Laor (2005) plot the C IV/H $\beta$  flux ratio against continuum slope and find evidence for reddening amounting to several tenths dex in the line ratio. Even if it does not correlate significantly with  $T_{\max}$ , reddening of this magnitude would significantly alter the relationship of the observed colors and disk models, as in our Fig. 3. Willott (2005) argues that the reddening curve proposed by Gaskell et al. is affected by selection biases relating to the composite spectra used. Higher redshift objects define the short wavelength part of the composite, and there may be a selection for lower extinction at higher redshift because of the limiting magnitude of the survey providing objects for the composite. Such a bias might affect our results, which use higher redshift objects for  $r_{21}$ . However, this bias would cause the extinction to be lower for  $r_{21}$  than  $r_{42}$ , opposite to the result in Fig. 3.

Baker (1997) finds that the radio-loud quasars (RLQs) are redder for more edge-on inclinations. Wills & Browne (1986) find broader emission lines in RLQs seen more edge-on, as would occur if H $\beta$  lines were emitted from a disk-like structure. This would result in broader lines for more edge-on disks, and greater reddening for broader lines. This is opposite to the trends in Fig. 3. While most SDSS QSOs are radio quiet, the same reasoning should apply. The relationship between nuclear gas supply and luminosity is uncertain. Plausibly, more abundant gas might lead to greater reddening as well as greater fueling and higher values of  $L_{\text{bol}}$  and  $T_{\max}$ .



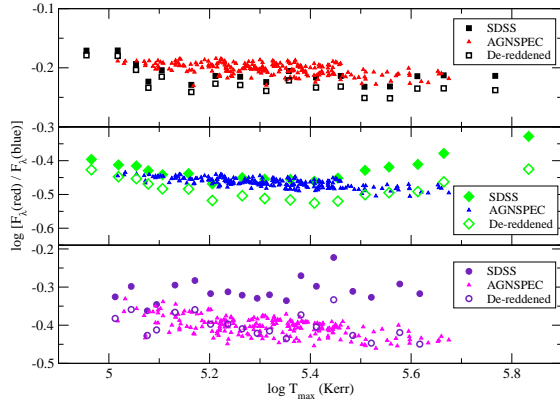


FIG. 6.— The binned observed points of Fig. 3 de-reddened with an SMC extinction curve. We assume here that the difference in the 2200 Å/1350 Å flux ratio between the observed points and the models is accounted for by reddening correlated with broad line-width. The other two flux ratios are then de-reddened by the corresponding amount according to the SMC extinction curve (see text).

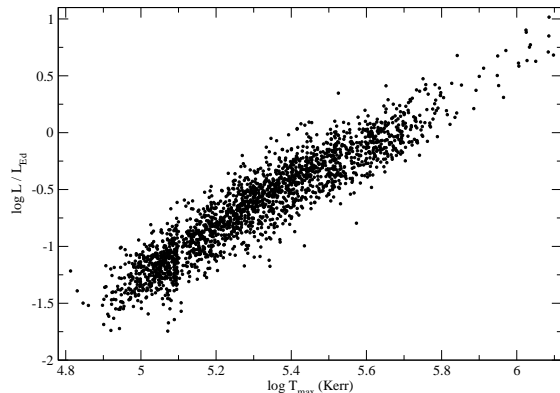


FIG. 7.— The Eddington ratio (in log). For higher redshift objects where  $\lambda 5100$  is inaccessible, we scale the 4000 Å continuum to 5100 Å as a power law with  $\alpha_\nu = -0.44 \pm 0.1$  (Vanden Berk et al. 2001). The uncertainty has only a  $\sim 1\%$  affect on the derived  $M_{\text{BH}}$  and  $L_{\text{bol}}/L_{\text{Ed}}$ .

### 3.4. Disk physics

Does accretion disk physics underly the difference between observed colors and the models? Figure 7 shows the strong correlation of  $T_{\text{max}}$  and  $L_{\text{bol}}/L_{\text{Ed}}$  for our sample, largely reflecting the fact that lower  $T_{\text{max}}$  objects have broader lines, and hence larger black holes. (Note that the derived  $L_{\text{bol}}/L_{\text{Ed}}$  is proportional to the bolometric correction  $f_L$  that we have assumed). Collin & Huré (2001) and Collin et al. (2002) have discussed high Eddington ratios in AGN based on objects with measured reverberation masses for the black hole. They note the possible role of slim disks or non-standard disks in super-Eddington accretion scenarios. The largest accretion rates correspond to the narrowest broad lines, particularly in NLS1 objects. In Fig. 3, the common NLS1 definition  $\text{FWHM} \leq 2000 \text{ km s}^{-1}$  corresponds to  $\log T_{\text{max}} \gtrsim 5.6$ .

Comparing Fig. 7 with Fig. 3, we see that the deviation

of  $r_{42}$  from the models occurs for  $L_{\text{bol}}/L_{\text{Ed}} > 0.3$  absent significant reddening (see above). This is just the range where the inner disk is severely thickened by radiation pressure, and departures from a thin disk geometry and atmospheric structure might be expected. The concept of “slim” accretion disks (Abramowicz et al. 1988) may therefore be relevant. These models modify the standard equations for thin accretion disks (Shakura & Sunyaev 1973) by including terms allowing for the radial pressure gradient and radial advection of heat. Szuszkiewicz, Malkan, & Abramowicz (1996) discuss the application of slim disks to AGN energy distributions, including the soft X-ray excess often observed in AGN (e.g., Turner & Pounds 1989). Slim disks are thin at large radius, and then increasingly depart from the thin disk solution at smaller radii as the local radiation flux counteracts the vertical gravity and thickens the disk. Slim disks thicken at a transition radius  $r_{\text{slim}}$  that increases with  $L_{\text{bol}}/L_{\text{Ed}}$ . Thus, longer wavelength radiation, emitted from the cooler, outer disk may obey the thin disk solution, while shorter wavelengths originating at smaller radii depart from the thin disk prediction. We attempted to estimate the effect of a slim accretion disk by applying an inner cutoff to the disk at the radius where the ratio of disk height to radius is  $H/R \approx 0.5$  (see discussion of  $H/R$  in Hubeny et al. 2000 and Laor & Netzer 1989). This is based on the idea that the locally radiated flux and effective temperature may be depressed at radii where advection carries energy inward. The  $L_\lambda(5100)/L_\lambda(4000)$  ratios are relatively unaffected by an inner disk cutoff; however, the color ratios,  $r_{42}$  and  $r_{21}$  do show an upward trend at higher  $T_{\text{max}}$ . Although they do not reproduce the correct magnitude of the ratios,  $r_{42}$  and  $r_{21}$  show a flat or ‘U’-shaped curve. The result of this simple approximation suggests that an accurate simulation of slim accretion disks could illuminate our observations of objects with high Eddington ratio.

Comptonization can affect the observed spectra of AGN, involving either an hot corona overlying the disk or electron scattering in the atmosphere itself (Shang et al. 2005; Hubeny et al. 2001; and references therein). The disk models here do not include Comptonization. Blaes et al. (2001), in a study of accretion disk models of 3C 273, find that Comptonization in the atmosphere does not affect the optical and mid-UV spectrum. Nevertheless, Comptonization should be kept in mind in studies of the QSO energy distribution.

We have considered only the optical and ultraviolet energy distribution. The statistical sampling allowed by SDSS makes it possible to study fairly subtle trends in the colors with  $T_{\text{max}}$ . Nevertheless,  $T_{\text{max}}$  has a much larger effect on the flux at short wavelengths. Laor et al. (1997) discuss the soft x-ray properties of AGN. They find that accretion disk models, for reasonable distributions of  $M_{\text{BH}}$  and  $\dot{M}$ , predict a larger range of optical to soft x-ray slope  $\alpha_{ox}$  than is observed. Our Figures 3 and 4 likewise show a smaller range of color in the observations than in the models.

Boroson and Green (1992) identified a number of correlations between observable properties of QSOs, the strongest of which they designated “Eigenvector 1”. This includes a tendency for stronger permitted Fe II broad line emission together with weaker narrow [O III] lines.

Boroson and Green suggested that Eigenvector 1 was driven by Eddington ratio, in the sense of increasing Fe II with increasing  $L_{\text{bol}}/L_{\text{Ed}}$ . This relationship was confirmed by Boroson (2002), but the physical causes remain unclear. The correlation of  $L_{\text{bol}}/L_{\text{Ed}}$  with  $T_{\text{max}}$  suggests that  $T_{\text{max}}$  may play a role in the physics underlying Eigenvector 1.

We are greatly indebted to Ivan Hubeny for making available the AGNSPEC code, which includes the program KERRTRANS of Eric Agol to calculate the relativistic transfer function. We thank Shane Davis, Robert Antonucci, Omer Blaes, Mike Brotherton, Ivan Hubeny, Pamela Jean, Zhaohui Shang, and Bev Wills for helpful discussions and assistance. EWB is supported by Marie Curie Incoming European Fellowship contract MIF1-CT-2005-008762 within the 6th European Community Framework Programme. This research was supported in part by the National Science Foundation under Grants No. PHY99-07949 and AST-0098594, and in part by the

Texas Advanced Research Program under grant 003658-0177-2001.

Funding for the Sloan Digital Sky Survey (SDSS) has been provided by the Alfred P. Sloan Foundation, the Participating Institutions, the National Aeronautics and Space Administration, the National Science Foundation, the U.S. Department of Energy, the Japanese Monbukagakusho, and the Max Planck Society. The SDSS Web site is <http://www.sdss.org/>. The SDSS is managed by the Astrophysical Research Consortium (ARC) for the Participating Institutions. The Participating Institutions are The University of Chicago, Fermilab, the Institute for Advanced Study, the Japan Participation Group, The Johns Hopkins University, the Korean Scientist Group, Los Alamos National Laboratory, the Max-Planck-Institute for Astronomy (MPIA), the Max-Planck-Institute for Astrophysics (MPA), New Mexico State University, University of Pittsburgh, University of Portsmouth, Princeton University, the United States Naval Observatory, and the University of Washington.

## REFERENCES

- Abramowicz, M. A., Czerny, B., Lasota, J. P., & Szuszkiewicz, E. 1988, *ApJ*, 332, 646
- Antonucci, R. 1999, in *High Energy Processes in Accreting Black Holes*, ASP Conference Series 161, ed. Juri Poutanen & Roland Svensson, p.193 (astro-ph/9810067)
- Antonucci, R. R. J.; Miller, J. S. 1985, *ApJ*, 297, 621
- Baker, J. C. 1997, *MNRAS*, 286, 23
- Baskin, A. & Laor, A. 2005, *MNRAS*, 356, 1029
- Bentz, M. C., Peterson, B. M., Pogge, R. W., Vestergaard, M., & Onken, C.A. 2006, *ApJ*, 644, 133
- Blaes, O. 2004, in *AGN Physics with the Sloan Digital Sky Survey*, ed. G.T. Richards and P. B. Hall, ASP Conference Series, 311, 1
- Blaes, O., Hubeny, I., Agol, E., & Krolik, J. H. 2001, *ApJ*, 563, 560
- Boroson, T. A. 2002, *ApJ*, 565, 78
- Boroson, T. A. & Green, R. F. 1992, *ApJS*, 80, 109
- Cheng, L., Shields, G. A., & Gebhardt, K. 2004, *BAAS*, 36, 767
- Coleman, H., & Shields, G. A. 1990, *ApJ*, 363, 415
- Collin, S. 1991, *A&A*, 249, 344
- Collin, S., Boisson, C., Mouchet, M., Dumont, A.-M., Coupé, S., Porquet, D., Rokaki, E. 2002, *A&A*, 388, 771
- Collin, S., & Huré, J.-M. 2001, *A&A*, 372, 50
- Comastri, A., Setti, G., Zamorani, G., Elvis, M., Wilkes, B. J., McDowell, J. C., Giommi, P. 1992, *ApJ*, 384, 62
- Constantin, A. & Shields, J. 2004, in *AGN Physics with the Sloan Digital Sky Survey*, ed. G.T. Richards and P. B. Hall, ASP Conference Series, 311, 269
- Cunningham, C. T. 1975, *ApJ*, 202, 788
- Czerny, B., Loska, Z., Szczerba, R., Cukierska, J., Madejski, G. 1995, *Acta Astron.*, 45, 623
- Dietrich, M., Hamann, F., Shields, J. C., Constantin, A., Vestergaard, M., Chaffee, et al. 2002, *ApJ*, 581, 912
- Gammie, C. F., Shapiro, S. L., & McKinney, J. C. 2004, *ApJ*, 602, 312
- Gaskell, C. M., Goosmann, R. W., Antonucci, R. R. J., Whysong, D. H. 2004, *ApJ*, 616, 147
- Gebhardt, K., et al. 2000a, *ApJ*, 539, L13
- Gebhardt, K., et al. 2000b, *ApJ*, 543, L5
- Greene, J. E., & Ho, L. C. 2005, *ApJ*, 627, 721
- Hopkins, P. F., Strauss, M. A., Hall, P. B., Richards, G. T., Cooper, A. S., Schneider, D. P., Vanden Berk, D. E., Jester, S., Brinkmann, J., Szokoly, G. P. 2004, *AJ*, 128, 1112
- Hubeny, I., Agol, E., Blaes, O., & Krolik, J. H. 2001, *ApJ*, 533, 710
- Hubeny, I., Blaes, O., Krolik, J. H., Agol, E. 2001, *ApJ*, 559, 680
- Hughes, S. A. & Blandford, R. D. 2003, *ApJ*, 585, 101
- Kaspi, S., Smith, P. S., Netzer, H., Maoz, D., Jannuzi, B. T., & Givon, U. 2000, *ApJ*, 533, 631
- Kaspi, S., Maoz, D., Netzer, H., Peterson, B. M., Vestergaard, M., & Jannuzi, B. T. 2005, *ApJ*, 629, 61
- Kishimoto, M., Antonucci, R., & Blaes, O. 2005, *MNRAS*, 364, 640
- Koratkar, A., & Blaes, O. 1999, *PASP*, 111, 1
- Kormendy, J. & Gebhardt, K. 2001, *AIP Conf. Proc.* 586: 20th Texas Symposium on relativistic astrophysics, 586, 363
- Laor, A., & Netzer, H. 1989, *MNRAS*, 238, 897
- Laor, A., Fiore, F. Elvis, M., Wilkes, B. J., McDowell, J. C. 1997, *ApJ*, 477, 93
- Malkan, M. 1983, *ApJ*, 268, 582
- McLure, R. J. & Dunlop, J. S. 2004, *MNRAS*, 352, 139
- McLure, R. J., & Jarvis, M. J. 2002, *MNRAS*, 337, 109
- Marziani, P., Sulentic, J. W., Zamanov, R., Calvani, M., Dultzin-Hacyan, D., Bachev, R., & Zwitter, T. 2003, *ApJS*, 145, 199
- Nelson, C. H. 2000, *ApJ*, 544, L91
- Novikov, I. E., & Thorne, K. S. 1973, in *Black Holes*, Les Houches, ed. C. DeWitt & B. DeWitt (New York: Gordon & Breach).
- Pei, Y. C. 1992, *ApJ*, 395, 130
- Pinkney, J., Gebhardt, K., Bender, R., Bower, G., Dressler, A., Faber, S. M., Filippenko, A. V., et al. 2003, *ApJ*, 596, 903
- Richards, G. T., Hall, P. B., Vanden Berk, D. E., Strauss, M. A., Schneider, D. P., Weinstein, M. A., et al. 2003, *AJ*, 126, 1131
- Richards, G. T., Lacy, M., Storrie-Lombardi, L. J., Hall, P. B., Gallagher, S. C., Hines, D. C., Fan, X., Papovich, C. et al. 2006, *ApJS*, 166, 470
- Salviander, S., G. A. Shields, K. Gebhardt, E. Bonning 2006, *ApJ in press*.
- Scott, J. E., Kriss, G. A., Brotherton, M., Richard F., Hutchings, J., Shull, J. M., Zheng, W. 2004, *ApJ*, 615, 135
- Shakura, N. I., & Sunyaev, R. A. 1973 *A&A*, 24, 337
- Shang, Z., Brotherton, M. S., Green, R. F., Kriss, G. A., Scott, J., Quijano, J. K., et al. 2005, *ApJ*, 619, 41
- Shields, G. A. 1989, *New York Academy Sciences Annals*, 571, 110
- Shields, G. A., Gebhardt, K., Salviander, S., Wills, B. J., Xie, B., Brotherton, M. S., Yuan, J., & Dietrich, M. 2003, *ApJ*, 583, 124
- Sun, W.-H. & Malkan, M. A. 1989, *ApJ*, 346, 68S
- Szuszkiewicz, E., Malkan, M. A., Abramowicz, M. A. 1996, *ApJ*, 458, 474
- Thorne, K. S. 1974, *ApJ*, 191, 507
- Tremaine, S., et al. 2002, *ApJ*, 574, 740
- Turner, T. J., & Pounds, K. A. 1989, *MNRAS*, 240, 833
- Vanden Berk, D. E., et al. 2001, *AJ*, 122, 549
- Vestergaard, M., & Wilkes, B. J. 2001, *ApJS*, 134, 1
- Volonteri, M., Madau, P., Quataert, E., Rees, M. 2005, *ApJ*, 620, 69
- Wandel, A., Peterson, B. M., & Malkan, M. A. 1999, *ApJ*, 526, 579
- Wandel, A. 1999, *ApJ*, 527, 649
- Wilkes, B. J. & Elvis, M. 1987, *ApJ*, 323, 243
- Wilkes, B. J., Kuraszkiewicz, J., Green, P. J., Mathur, S. and McDowell, J. C. 1999, *ApJ*, 513, 76
- Willott, C. J. 2005, *ApJ*, 627, L101
- Wills, B. J. & Browne, I. W. A. 1986, *ApJ*, 302, 56